

Quantum Critical Behaviour in a Graphene-like Model

Simon Hands^a and Costas Strouthos^b

^a*Department of Physics, Swansea University,
Singleton Park, Swansea SA2 8PP, U.K.*

^b*Department of Mechanical Engineering, University of Cyprus,
Nicosia 1678, Cyprus.*

Abstract: We present the first results of numerical simulations of a 2+1 dimensional fermion field theory based on a recent proposal for a model of graphene, consisting of N_f four-component Dirac fermions moving in the plane and interacting via an instantaneous Coulomb interaction. In the strong-coupling limit we identify a critical number of flavors $N_{fc} = 4.8(2)$ separating an insulating from a conducting phase. This transition corresponds to the location of a quantum critical point, and we use a fit to the equation of state for the chiral order parameter to estimate the critical exponents. Next we simulate $N_f = 2$ corresponding to real graphene, and approximately locate a transition from strong to weak coupling behaviour. Strong correlations are evident in the weak-coupling regime.

PACS: 11.10.Kk, 11.15.Ha, 71.10.Fd, 73.63Bd

Keywords: graphene, lattice model, quantum critical point

1 Introduction

While there has been considerable recent interest in graphene sparked by its discovery and subsequent experimental study [1], the remarkable properties of electronic systems on two-dimensional honeycomb lattices have been suspected for many years [2]. In brief, for a carbon monolayer having one mobile electron per atom, a simple tight-binding model shows that the spectrum of low-energy excitations exhibits a linear dispersion relation centred on zeroes located at the six corners of the first Brillouin zone (eg. [3]). Using a linear transformation among the fields at two independent zeroes it is possible to recast the Hamiltonian in Dirac form with $N_f = 2$ flavors of four-component spinor ψ , the counting of the massless degrees of freedom coming from 2 C atoms per unit cell \times 2 zeroes per zone \times 2 physical spin components per electron. Electron propagation in the graphene layer is thus relativistic, albeit at a speed $v_F \approx c/100$. The implications for the high mobility of the resulting charge carriers (which may be negatively-charged “particles” or positively-charged “holes” depending on doping) is the source of the current excitement. The stability of the zero-energy points is topological in origin, as emphasised in [4].

While the above considerations apply quite generally, a realistic model of graphene must incorporate interactions between charge carriers. One such model due to Son [5] has N_f massless fermion flavors propagating in the plane, but interacting via an instantaneous $3d$ Coulomb interaction. In Euclidean metric and static gauge $\partial_0 A_0 = 0$ the action reads

$$S_1 = \sum_{a=1}^{N_f} \int dx_0 d^2x (\bar{\psi}_a \gamma_0 \partial_0 \psi_a + v_F \bar{\psi}_a \vec{\gamma} \cdot \vec{\nabla} \psi_a + iV \bar{\psi}_a \gamma_0 \psi_a) + \frac{1}{2e^2} \int dx_0 d^3x (\partial_i V)^2, \quad (1)$$

where e is the electron charge, $V \equiv A_0$ is the electrostatic potential, and the 4×4 Dirac matrices satisfy $\{\gamma_\mu, \gamma_\nu\} = 2\delta_{\mu\nu}$, $\mu = 0, 1, 2, 3$. In our notation \vec{x} is a vector in the $2d$ plane while the index i runs over all three spatial directions. Within the graphene layer, classical propagation of the potential is obtained by integrating over the perpendicular coordinate, yielding

$$D_0(p) = \frac{e^2}{2|\vec{p}|}. \quad (2)$$

To proceed, assume a large- N_f limit so that the dominant quantum correction $\Pi(p)$ comes from a vacuum polarisation fermion – antifermion loop. The resummed V propagator becomes

$$D_1(p) = (D_0^{-1}(p) - \Pi(p))^{-1} = \left(\frac{2|\vec{p}|}{e^2} + \frac{N_f}{8} \frac{|\vec{p}|^2}{(p^2)^{\frac{1}{2}}} \right)^{-1}, \quad (3)$$

where $p^2 = (p_0, \vec{p})^2 \equiv p_0^2 + v_F^2 |\vec{p}|^2$. In either the strong coupling or large- N_f limits $D_1(p)$ is thus dominated by the quantum correction, the relative importance of the original Coulomb interaction being governed by a parameter $\lambda \equiv |\Pi/D_0|_{p_0=0}$. Restoring SI units, we obtain

$$\lambda = \frac{e^2 N_f}{16\varepsilon_0 \hbar v_F} \simeq 1.7 N_f. \quad (4)$$

The form of the interaction (3) means that analytic methods are trustworthy in the large- N_f regime. For instance, in the strong coupling limit $e^2 \rightarrow \infty^1$ we expect a modification of the dispersion relation, such that the fermion energy is related to momentum via $\omega \propto p^z$, where z is a dynamical critical exponent predicted to take the value $z \simeq 1 - \frac{4}{\pi^2 N_f} \approx 0.8$ for $N_f = 2$ [5]. Ref. [5] in addition discusses the phase diagram of the graphene model (1) in the (N_f, e^{-2}) plane, and raises the possibility of symmetry breaking due to non-perturbative N_f^{-1} effects. The symmetry breaking, due to the spontaneous condensation of particle - hole pairs, is signalled by an order parameter $\langle \bar{\psi} \psi \rangle \neq 0$ – in relativistic field theory this is known as “chiral symmetry breaking”. Physically the most important outcome is the generation of a gap in the fermion spectrum, implying the model describes an insulator. Son postulates that this

¹In experiments it is only possible to *reduce* the effective electron charge by mounting the graphene layer on a dielectric substrate.

insulating phase exists in the corner of the phase diagram corresponding to large e^2 and small N_f , and in particular that the insulator-conductor phase transition taking place at $N_f = N_{fc}$ in the strong-coupling limit $e^2 \rightarrow \infty$ is a novel quantum critical point. The value of N_{fc} , and the issue of whether it is greater than or less than the physical value $N_f = 2$, must be settled by a non-perturbative calculation. A recent estimate, obtained by a renormalisation group treatment of radiatively-induced four-fermion contact interactions, is $N_{fc} = 2.03$ [6].

The proposed physics is very reminiscent of another $2+1d$ fermion model, this time relativistically covariant, namely the Thirring model with action

$$S_{Th} = \sum_{a=1}^{N_f} \int dx_0 d^2x \left[\bar{\psi}_a \gamma_\mu \partial_\mu \psi_a + \frac{g^2}{2} (\bar{\psi}_a \gamma_\mu \psi_a)^2 \right], \quad (5)$$

with $\mu = 0, 1, 2$, particularly once we insist on units such that $v_F = 1$. Note that in contrast to the graphene model the coupling g^2 has mass dimension -1. Once again, the model is analytically tractable at large N_f , but exhibits spontaneous chiral symmetry breaking leading to gapped fermions at small N_f and large g^2 [7, 8]. Arguably the Thirring model is the simplest field theory of fermions requiring a computational solution: the location of the phase transition at $N_f = N_{fc}$ in the strong coupling limit has recently been determined by lattice simulation to be $N_{fc} = 6.6(1)$ [9]. The apparent similarity of the two systems has led us to propose a Thirring-like model pertinent to graphene, with action

$$S_2 = \sum_{a=1}^{N_f} \int dx_0 d^2x \left[\bar{\psi}_a \gamma_\mu \partial_\mu \psi_a + \frac{g^2}{2} (\bar{\psi}_a \gamma_0 \psi_a)^2 \right]. \quad (6)$$

The only difference with (5) is that the contact interaction is now only between the time-like components of the fermion current, so that the model is no longer covariant.

The traditional way to proceed is to introduce an auxiliary boson field V . The resulting action

$$S'_2 = \sum_{a=1}^{N_f} \int dx_0 d^2x \left[\bar{\psi}_a \gamma_\mu \partial_\mu \psi_a + iV \bar{\psi}_a \gamma_0 \psi_a + \frac{1}{2g^2} V^2 \right] \quad (7)$$

reproduces the identical dynamics as (6) once V is integrated out. As for (1) we assume a large- N_f limit to estimate the dominant vacuum polarisation correction; the resultant propagator for V is

$$D_2(p) = \left(\frac{1}{g^2} + \frac{N_f}{8} \frac{|\vec{p}|^2}{(p^2)^{\frac{1}{2}}} \right)^{-1}. \quad (8)$$

In the strong-coupling or large- N_f limits, D_2 coincides with D_1 (3), implying that the fermion interactions are equivalent. It is also the case that $\lim_{p \rightarrow \infty} D_2(p) = \lim_{\lambda \rightarrow \infty} D_1(p)$.

This last limit is important because critical behaviour in the Thirring model (5) is governed by a UV-stable fixed point of the renormalisation group [7]. We anticipate that the model (6) is similar and expect its predictions, in particular for critical behaviour such as the value of N_{fc} , to be generally valid for Son's model (1) in the limit of large λ .

In the following section we present a version of the action (7) discretised on a space-time lattice, and outline how its dynamics can be investigated by standard Monte Carlo simulation techniques. To our knowledge this paper is the first to apply lattice gauge theory techniques to graphene. In this first paper we focus exclusively on the equivalent of the order parameter $\langle \bar{\psi}\psi \rangle$ in the (N_f, g^{-2}) plane. In Sec. 3.1 we explore the strong coupling limit and identify the critical flavor number N_{fc} , and then attempt to characterise the transition from insulator to conductor by studying the critical equation of state using finite volume scaling. In Sec. 3.2 we switch attention to the physical case $N_f = 2$, and present results from a study of $\langle \bar{\psi}\psi \rangle$ as a function of g^2 . A brief discussion of the implications for the graphene model of [5] follows.

2 Lattice Model and Simulation

The lattice model studied in this paper is closely related to the lattice Thirring model studied in [7]. It is written in terms of staggered lattice fermions, ie. single-component Grassmann fields $\chi, \bar{\chi}$ defined on the sites x of a three-dimensional cubic lattice, by the action

$$S_{latt} = \frac{1}{2} \sum_{x\mu a} \bar{\chi}_{ax} \eta_{\mu x} \left[(1 + \delta_{\mu 0} \sqrt{\frac{2g^2}{N}} e^{iV_x}) \chi_{ax+\hat{\mu}} - (1 + \delta_{\mu 0} \sqrt{\frac{2g^2}{N}} e^{-iV_{x-\hat{0}}}) \chi_{ax-\hat{\mu}} \right] + m \sum_{xa} \bar{\chi}_{ax} \chi_{ax}. \quad (9)$$

The flavor indices $a = 1, \dots, N$. The sign factors $\eta_{x\mu} \equiv (-1)^{x_0 + \dots + x_{\mu-1}}$ ensure that in the long-wavelength limit the the first (antihermitian) term in S_{latt} describes the Euclidean propagation of $N_f = 2N$ flavors of relativistic fermion described by four-component spinors [10]. The fermion mass term proportional to m has been added to provide a IR regulator for modes which would otherwise be massless; beyond the usual critical slowing down, it is important to stress that simulations directly in the limit $m \rightarrow 0$ present severe technical difficulties. The hopping terms in S_{latt} involve the auxiliary boson field V_x which is formally defined on the *timelike* links connecting sites x with $x + \hat{0}$. The N -dependence in the kinetic terms is conventional, and retained to ensure continuity with the studies of [7, 8, 9]. In order to compare with the formulation of the previous section the rescaling $g^2 \rightarrow Ng^2$ is required.

It can be shown that the action (9) can be reexpressed in terms of four-component spinors in a form similar but not identical to (6). For full details of the relation between the two actions we refer the reader to [7]. Here we merely note that the spontaneous generation of a condensate $\langle \bar{\chi}\chi \rangle \neq 0$ in the lattice model results in a chiral symmetry

breaking pattern $U(N)\otimes U(N)\rightarrow U(N)$, whereas in the continuum model (6) $\langle\bar{\psi}\psi\rangle\neq 0$ breaks $U(2N_f)\rightarrow U(N_f)\otimes U(N_f)$ [3]. A term proportional to m explicitly breaks the symmetry in either case. It is plausible that the effective global symmetry of the lattice model enlarges in the continuum limit, and the correct continuum pattern recovered. In what follows we will assume that the chiral symmetry breaking described by $\langle\bar{\chi}\chi\rangle\neq 0$ is equivalent to the metal-insulator transition.

The novelty of [9] was the first study of the Thirring model (5) by lattice means in the strong-coupling limit $g^2\rightarrow\infty$. Since we aim to repeat the strategy here we discuss how this was done. First, note that the vacuum polarisation calculation leading to the results (3,8) does not go through in quite the same way for the lattice regularised model (9); rather, there is an additive correction which is momentum independent and UV-divergent:

$$\Pi^{latt}(p)=\Pi^{cont}(p)+g^2J(m),\tag{10}$$

where $J(m)$ comes from incomplete cancellation of a lattice tadpole diagram [7]. This extra divergence not present in the continuum treatments can be absorbed by a wave-function renormalisation of V and a coupling constant renormalisation

$$g_R^2=\frac{g^2}{1-g^2J(m)}.\tag{11}$$

In the large- N_f limit we thus expect to find the strong coupling limit of the lattice model at $g_R^2\rightarrow\infty$ implying $g^2\rightarrow g_{lim}^2=J^{-1}(m)$. For $g^2>g_{lim}^2$ $D_{latt}(p)$ becomes negative, and S_{latt} no longer describes a unitary theory.

Away from the large- N_f limit, where chiral symmetry may be spontaneously broken, there is no analytical criterion for identifying g_{lim}^2 ; however in this case a numerical calculation of $\langle\bar{\chi}\chi\rangle$ shows a clear peak at $g^2=g_{peak}^2$, whose location is approximately independent of both volume and m , indicating an origin at the UV scale [9]. Fig. 1 exemplifies this behaviour in the model (9) with $N_f=2$ on system volumes L^3 : for $L\geq 24$ we identify $1/g_{peak}^2\simeq 0.3$. Since for orthodox chiral symmetry breaking the magnitude of the condensate is expected to increase monotonically with the coupling strength, we interpret the peak as the point where unitarity violation sets in, ie. $g_{lim}^2\approx g_{peak}^2$. In the next section, we shall use simulations performed at $g^2=g_{peak}^2$ to explore the strong coupling limit, and find evidence for a chiral symmetry restoring phase transition at a well-defined N_{fc} .

Writing the action (9) in the form $\bar{\chi}_iM_{ij}\chi_j$, it is possible to integrate out the fermion fields analytically to yield the path integral

$$\mathcal{Z}_{latt}=\int\mathcal{D}V(\det M[V;m])^N.\tag{12}$$

Techniques to simulate the physics described by (12) typically proceed by evolving a boson configuration $\{V\}$ through a fictitious simulation time using a quasi-Hamiltonian dynamics in which quantum effects are incorporated via periodic stochastic refreshments.

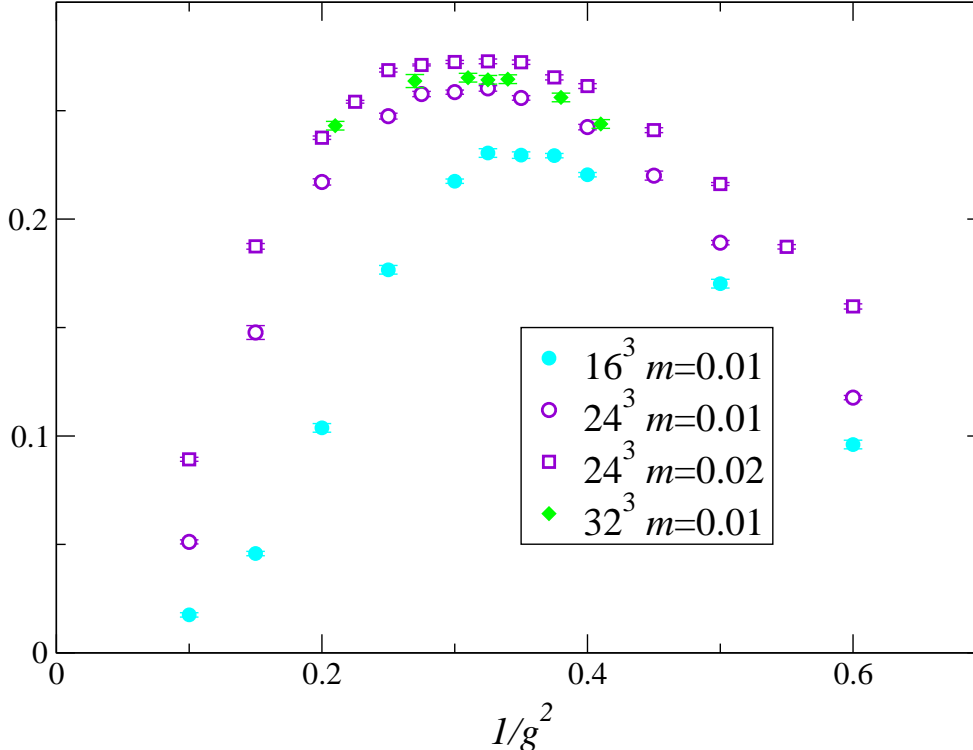


Figure 1: $\langle \bar{\chi}\chi \rangle$ vs. $1/g^2$ for $N_f = 2$.

We implement this using the hybrid molecular dynamics (HMD) algorithm [11]. The key step in the evolution involves the calculation of a force

$$-\frac{\delta S}{\delta V} = N \text{tr} M^{-1} \frac{\delta M}{\delta V}. \quad (13)$$

Since the force can be calculated for arbitrary N , it is possible to simulate the dynamics for non-integer N , which is equivalent to regarding the path integral (12) as the fundamental definition of the model. Of course, only for integer N , and therefore for even integer N_f , is it possible to express the theory as a local action in the fermion variables $\chi, \bar{\chi}$.

In the simulations described in this paper we used a HMD algorithm to perform simulations with arbitrary N_f . In principle, this method is not exact in the sense that results have a systematic dependence on the discrete timestep $\Delta\tau$ used to integrate the HMD equation of motion. We have used $\Delta\tau = 0.0025$ on the smallest systems (16^3 , 24^3 , 32^3), $\Delta\tau = 0.00125$ on $16^2 \times 48$ and $\Delta\tau = 0.000625$ on $16^2 \times 64$; in all cases we checked that the resulting systematic error is smaller than the statistical error. The mean trajectory length $\bar{\tau} = 1.0$, and $\langle \bar{\chi}\chi \rangle$ measured using 10 stochastic estimators after every trajectory. Roughly 200-400 trajectories were generated for $16^2 \times 48, 64$, 600 for $24^3, 32^3$ and $O(1000)$ for 16^3 . Further details of the numerical methods used can be found in [7, 8].

3 Results

We performed simulations on system volumes $L_s^2 \times L_t = 16^3, 24^3$ and 32^3 , using fermion masses $m = 0.01, \dots, 0.04$. Because the action (9) does not treat spacelike and timelike directions equivalently, we also found it useful to explore the consequences of independently varying L_s and L_t , and thus in addition studied $16^2 \times 48, 64$; $24^2 \times 32, 48$; and $32^2 \times 24$. As we shall see, the anisotropic nature of the model's dynamics results in the systematic effects due to finite L_t being much more important than those due to finite L_s . The only observable discussed in this initial study is the chiral condensate $\langle \bar{\chi}\chi \rangle \equiv \langle \text{tr}M^{-1} \rangle$.

3.1 Strong Coupling Limit

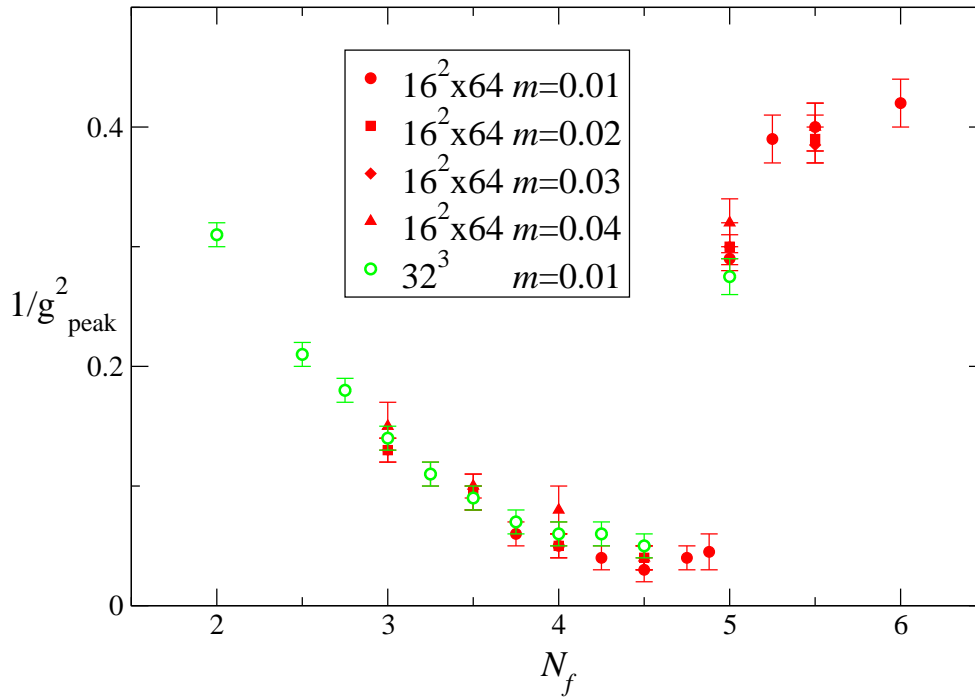


Figure 2: $1/g_{\text{peak}}^2$ vs. N_f .

As described above, to explore the strong coupling limit $g_R^2 \rightarrow \infty$ we made the ansatz $g^2 = g_{\text{peak}}^2$, where g_{peak}^2 denotes the location of the peak in $\langle \bar{\chi}\chi \rangle$ at given N_f . Fig. 2 shows $1/g_{\text{peak}}^2(N_f)$ for some representative lattice volumes and fermion masses, confirming that its value, arising as it does from UV lattice artifacts, is to good approximation volume and mass independent. The behaviour is qualitatively similar to that found for the strong-coupling Thirring model shown in Fig. 3 of [9]. We see that $1/g_{\text{peak}}^2$ decreases as N_f increases from 2 to 4.75, at which point the curve reaches a minimum. There is then a steep increase at $N_f \approx 4.9$ followed by a levelling off, implying a significant change

in the model's strong coupling behaviour. Our interpretation, to be supported below by a study of the equation of state, is that for N_f below the change the model is in a chirally broken phase, and that above the change chiral symmetry is restored, implying $\lim_{m \rightarrow 0} \langle \bar{\chi} \chi \rangle = 0$. Using this criterion we identify the critical flavor number for chiral symmetry restoration in the strong coupling limit, with a conservative error, as

$$N_{fc} = 4.8(2). \quad (14)$$

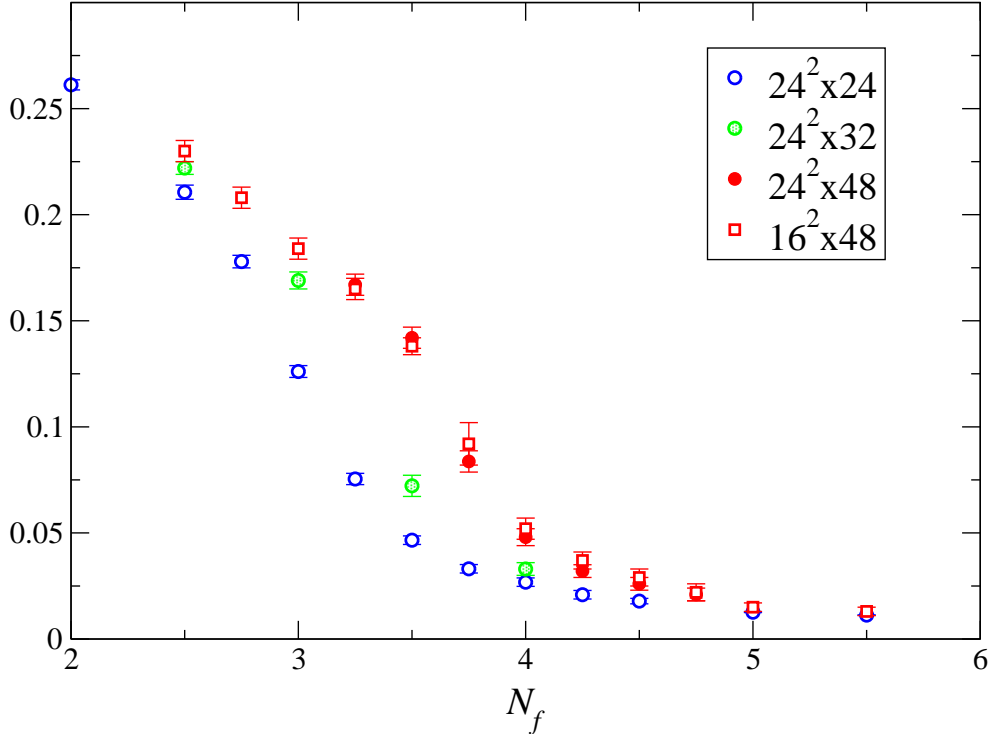


Figure 3: $\langle \bar{\chi} \chi \rangle$ vs. N_f at $m = 0.01$ on various lattice volumes.

In the rest of this section we analyse data taken at $g^2 = g_{\text{peak}}^2$ in an attempt to determine the critical equation of state $\langle \bar{\chi} \chi(m, N_f) \rangle$ in the strong coupling limit. Note that typically 4 – 6 independent simulations were used to identify g_{peak}^2 for each N_f . In the thermodynamic zero temperature limit, a simple ansatz for the approximate scaling behaviour close to a quantum critical point is given by

$$m = A(N_f - N_{fc}) \langle \bar{\chi} \chi \rangle^p + B \langle \bar{\chi} \chi \rangle^\delta, \quad (15)$$

whence $\langle \bar{\chi} \chi \rangle|_{N_f=N_{fc}} \propto m^{\frac{1}{\delta}}$ and the conventional exponent in $\langle \bar{\chi} \chi \rangle|_{m=0} \propto (N_{fc} - N_f)^\beta$ for $N_f < N_{fc}$ is given by $\beta = (\delta - p)^{-1}$. We must, however, take account of the fact that our data is taken on finite systems. Fig. 3 shows data for $m = 0.01$ from various lattices: a comparison between $16^2 \times 48$ and $24^2 \times 48$ demonstrates that the dominant finite volume effects are due to varying L_t , while the effects of finite L_s are negligible for $L_s \geq 16$.

The theory of finite volume effects in models such as (9) with anisotropic correlations is outlined in [12]. Near a critical point it is possible in principle to distinguish two correlation lengths ξ_s and ξ_t , each diverging with a distinct critical exponent ν_s , ν_t as $N_f \rightarrow N_{fc}$. In d spacetime dimensions these are related to conventionally-defined exponents governing scaling of the order parameter and its associated susceptibility via a generalised hyperscaling relation

$$\nu_t + (d - 1)\nu_s = \gamma + 2\beta. \quad (16)$$

Motivated by Fig. 3, in our analysis we take a pragmatic approach and assume all volume effects are due to finite L_t . The ansatz for the modified equation of state, inspired by a renormalisation group analysis [7] is then

$$m = A[(N_f - N_{fc}) + CL_t^{-\frac{1}{\nu_t}}]\langle\bar{\chi}\chi\rangle^p + B\langle\bar{\chi}\chi\rangle^\delta; \quad (17)$$

we fit this form to our dataset with a least squares fit. Our complete dataset contains 124 data taken at various N_f , m , L_s , L_t (recall the value of $1/g_{\text{peak}}^2$ must be independently determined for each parameter set, so the simulation effort involved is considerable; approximately 100 000 processor hours using 2.4GHz Opteron were required).

Experience with previous models shows that the fitted equation of state is very sensitive to assumptions made about the scaling window (ie. the ranges of N_f and m to include in the fit), and the smallest volume to include in the scaling ansatz (17). For this reason we judge it best to present a compilation of different fits in Table 1. We

| fit | # | A | B | N_{fc} | δ | p | C | ν_t | χ^2/dof |
|----------------------------|----|----------|----------------------|----------|----------|---------|----------|----------|---------------------|
| Power, | 28 | 0.31(3) | 41.5(15) | 3.81(3) | 3.96(3) | 0.87(3) | – | – | 4.8 |
| Power, $m \geq 0.02$ | 18 | 0.30(7) | 87(55) | 3.87(9) | 4.4(4) | 0.82(6) | – | – | 5.9 |
| Power, $m \geq 0.03$ | 12 | 2.1(10) | 3800(18) | 4.3(1) | 6.0(1) | 1.3(1) | – | – | 6.4 |
| FVS, $m = 0.01$ | 53 | 1.5(7) | 63(22) | 4.60(15) | 3.9(1) | 1.3(1) | 9.7(10) | 1.7(2) | 4.0 |
| as above $L_t \geq 24$ | 48 | 4.5(32) | 161(97) | 4.95(16) | 4.0(1) | 1.6(2) | 7.9(5) | 2.1(2) | 4.0 |
| as above $N_f < 4.5$ | 46 | 712(100) | $2.3(3) \times 10^4$ | 4.46(9) | 5.25(4) | 3.00(4) | 15(3) | 1.2(1) | 5.4 |
| FVS, all m | 96 | 0.23(1) | 19(2) | 3.85(4) | 4.03(8) | 0.88(1) | 17.5(17) | 1.10(5) | 6.3 |
| as above $L_t \geq 32$ | 70 | 0.20(1) | 10.5(1) | 4.7(3) | 3.6(1) | 0.82(2) | 6.0(6) | 2.6(8) | 5.1 |
| as above $N_f \geq 3$ | 60 | 0.21(1) | 237(106) | 4.6(7) | 5.5(3) | 0.86(2) | 8.1(34) | 2.1(1.1) | 3.1 |
| $N_f \geq 3$ $L_t \geq 24$ | 75 | 0.21(1) | 352(137) | 4.1(1) | 5.8(2) | 0.87(2) | 15(4) | 1.3(2) | 3.4 |
| FVS, $m \geq 0.02$ | 43 | 0.19(2) | 10.4(18) | 3.76(11) | 3.55(13) | 0.78(3) | 24(15) | 0.9(2) | 7.3 |
| as above $L_t \geq 32$ | 32 | 0.16(2) | 6.5(14) | 3.9(4) | 3.21(15) | 0.72(4) | 12(19) | 1.2(9) | 6.4 |

Table 1: Various fits to the Equations of State (15) “Power” and (17) “FVS”

tried fits to both the “Power” equation of state (15), with 5 free parameters, using data from a single lattice size $16^2 \times 64$, and fits using the finite- L_t “FVS” scaling form (17) with 7 free parameters.² In the latter case data with $N_f \geq 5$ was excluded from the fit

²Note it is not possible to use hyperscaling to constrain the value of ν_t , as done in [7, 8, 9].

because their small errorbars destabilised the fits; since this data probably comes from the chirally symmetric phase there may be a small systematic error in the identification of g_{peak}^2 across the transition.

Fits to (15) favour $N_{fc} \simeq 3.8 - 4$, and $p \simeq 0.9$. These values are also favoured by the most comprehensive FVS fit to the 96 datapoints with $N_f < 5$. There is no evidence that discarding $m = 0.01$ data, which may be most prone to finite volume artifacts, improves any of the fits. On the other hand, discarding $L_t = 16$ and perhaps $L_t = 24$ does have a significant effect on the fitted values of N_{fc} , p and ν_t in the FVS fits. In these cases the fitted $\delta \approx 4$. However, once data with extremal values of N_f is excluded, on the assumption that they lie outside the scaling window, the fitted values of δ rise to $\gtrsim 5$. In almost all cases the fitted value of ν_t exceeds 1, though often not by a statistically significant margin.

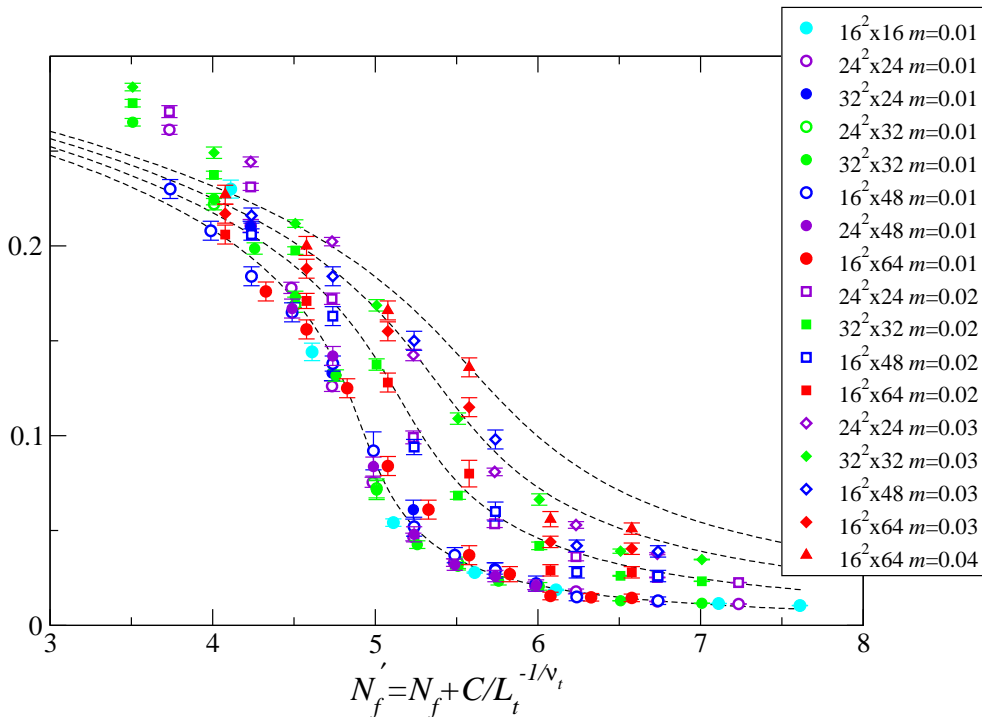


Figure 4: Finite volume scaling fit to (17) to data with $m = 0.01$ (circles), 0.02 (squares), 0.03 (diamonds) and 0.04 (triangles), in terms of N'_f .

Our favourite fit, yielding the smallest χ^2/dof , emerges from the 60 datapoints with $N_f \in [3, 5)$ and $L_t \geq 32$. Another reason for preferring this is that the fitted N_{fc} is consistent with the value (14) coming from the behaviour of $g_{\text{peak}}^2(N_f)$, which could be regarded as an additional constraint on the global fit. The fit is plotted in Fig. 4 in terms of the control parameter in the thermodynamic limit $N'_f = N_f + CL_t^{-\frac{1}{\nu_t}}$, so that data with differing L_t should collapse onto a single curve for each value of m .

To summarise: this “best” fit provides a reasonable description of the data in the window $4.5 \lesssim N'_f \lesssim 6$, in particular for the smallest mass $m = 0.01$; fits of the form

(17) are capable of yielding a fitted N_{fc} consistent with (14); and the preferred value of $\nu_t \approx 2$ once this consistency criterion is applied.

3.2 $N_f = 2$

Next we turn our attention to the physical case $N_f = 2$. Since $N_{fc} > 2$, we expect chiral symmetry to be broken at strong coupling and potentially restored at some finite g_R^2 . Accordingly we study $\langle \bar{\chi}\chi \rangle$ as a function of $1/g^2$ and here study additional values of the mass parameter m . Our results are summarised in Fig 5.

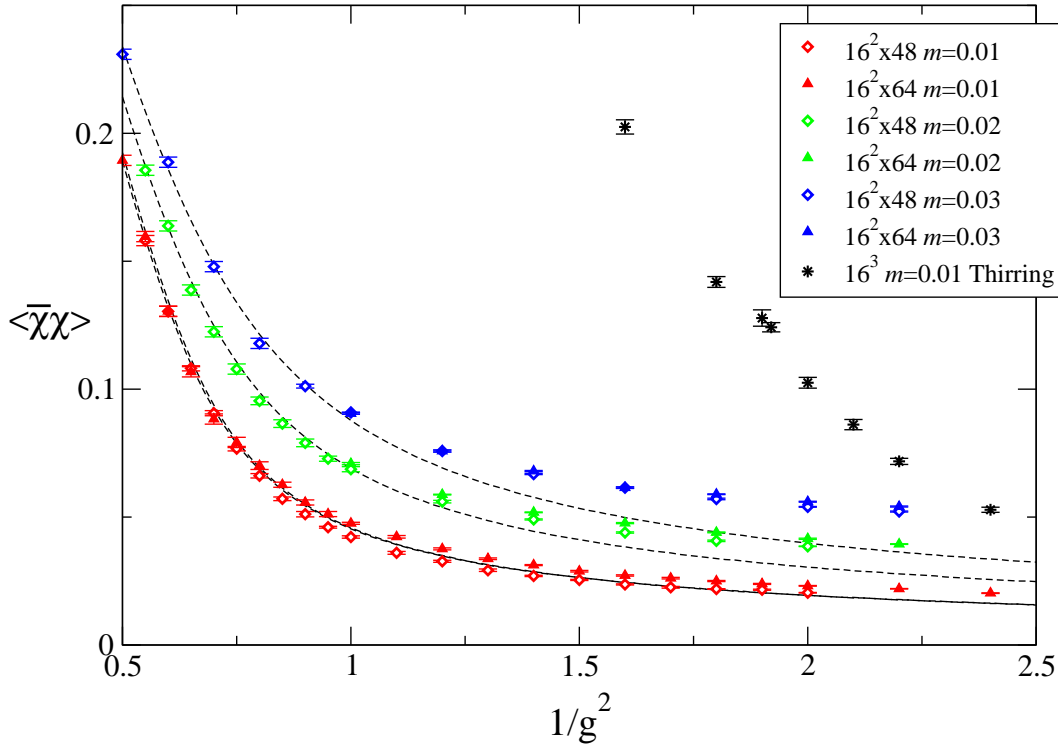


Figure 5: $\langle \bar{\chi}\chi \rangle$ vs. $1/g^2$ for $N_f = 2$.

As before, we have attempted to fit a critical equation of state using the forms (15) to data from $16^2 \times 64$, and (17), in each case replacing $(N_f - N_{fc})$ with $(g^{-2} - g_c^{-2})$. No stable fits were found unless data with $1/g^2 \lesssim 1$ were excluded. Our most comprehensive fit, using the FVS form and restricting the data to $L_t \geq 48$, $1/g^2 \leq 0.9$, yields $1/g_c^2 = 0.632(6)$ and is shown in the figure. All the fits we found identify a $1/g_c^2 \simeq 0.6 \gg 1/g_{\text{peak}}^2$, but all clearly undershoot the data at weaker couplings by a considerable margin. We conclude that the equation of state ansatz (15,17) are inadequate to describe the data.

Instead, we will distinguish between a “strong coupling” regime $1/g^2 \lesssim 0.75$ where $\langle \bar{\chi}\chi \rangle$ is numerically large and finite volume effects are negligible and a “weak coupling” regime $1/g^2 \gtrsim 0.75$ where the opposite holds true. Two comments about the weak coupling regime are worth making. First, as is clear from Figs. 5 and 6, finite volume effects

are unexpectedly large, and indeed increase in relative importance until $1/g^2 \gtrsim 1$; it is this feature which has made a global FVS fit impossible. In a conventional symmetry-breaking scenario by contrast one expects the finite volume effects to be larger in the broken phase, where there are long-range correlations due to Goldstone bosons. Secondly, in a chirally symmetric phase one expects $\langle \bar{\chi}\chi \rangle \propto m$ for small m and weak interactions; inspection of the data plotted in Fig. 6 appears to imply either that a linear extrapolation to $m \rightarrow 0$ would yield a non-vanishing order parameter, or alternatively, that chiral symmetry restoration for these values of $g^2 < g_c^2$ would require $\langle \bar{\chi}\chi(m) \rangle$ to

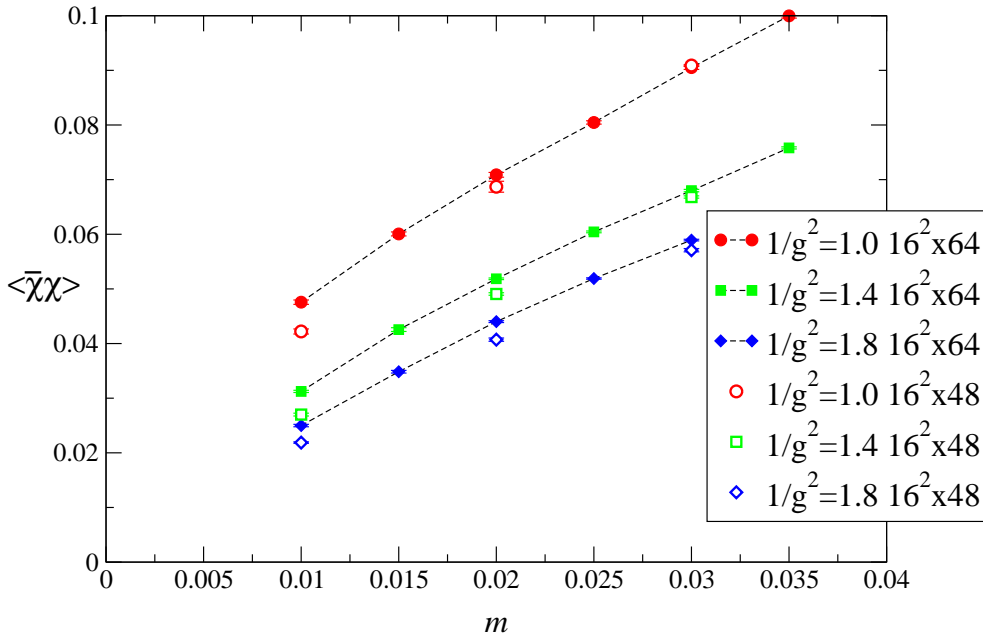


Figure 6: $\langle \bar{\chi}\chi \rangle$ vs. m for $N_f = 2$ in the weak-coupling regime.

exhibit some negative curvature, for which there is some tentative evidence in the figure. We conclude that either chiral symmetry remains broken at weak coupling, or that there are long-range correlations in this region.

We briefly consider alternative scaling scenarios. In the chiral and thermodynamic limits two other kinds of behaviour are possible to envisage, and are not currently excluded by our data. Firstly, a form $\langle \bar{\chi}\chi \rangle = Ae^{-B/g^2}$ would predict broken chiral symmetry for all g^2 . This is barely credible, since the $\chi - \bar{\chi}$ forces in this model are weaker than for the $N_f = 2$ Thirring model, where two independent simulation studies find a second order chiral restoring transition at $1/g^2 \simeq 1.9$ [7, 13] (Fig. 5 also shows Thirring data from 16^3 [7]). Second, $\langle \bar{\chi}\chi \rangle = Ae^{-B/(g_c^2 - g^2)^q}$ describes chiral symmetry restoration via an infinite order phase transition at $g^2 = g_c^2$. Without a reliable finite volume scaling hypothesis we cannot estimate g_c^2 , B or q . By analogy with the Kosterlitz-Thouless transition in $2d$ systems, though, this scenario predicts a critical and hence strongly fluctuating system for $g^2 > g_c^2$ which could plausibly account for the observations reported above.

4 Discussion

In this paper we studied a model (6) which has very similar properties, including the same global symmetries, as the graphene-related model recently proposed to describe quantum critical behaviour in the (N_f, e^2) plane [5]. Using a simulation strategy devised for the $2+1d$ Thirring model [9], we have identified the critical number of flavors separating insulating from conducting phases in the strong coupling limit to be $N_{fc} = 4.8(2)$. This implies that the strong coupling limit of graphene with $N_f = 2$ is an insulator. Since the properties of a critical point should be universal, we expect this result to be a robust prediction of our work, thus furnishing the first systematic non-perturbative prediction of quantum critical behaviour in this system. We also managed a reasonable fit of our strong-coupling data to an equation of state describing a continuous phase transition at the critical point, and obtained estimates for the critical exponents.

The fitted value of ν_t gives partial information about the nature of correlations in the vicinity of the fixed point. Substituting our favoured values $\delta = 5.5$, $p = 0.86$, $\nu_t = 2.1$ into (16), we obtain $\nu_s = \frac{1}{2}\gamma - 0.83$. Without studying the order parameter susceptibility we have no independent estimate of γ , but note that it would need to have a value of $O(6)$ in order for ν_s to exceed ν_t . Now, there is a further relation governing the scaling of critical correlation functions [12]:

$$(d - 2 + \eta_t)\nu_t = (d - 2 + \eta_s)\nu_s \quad \Rightarrow \quad \frac{\nu_t}{\nu_s} = \frac{1 + \eta_s}{1 + \eta_t}, \quad (18)$$

where order parameter correlations $\langle \bar{\chi}\chi(0)\bar{\chi}\chi(x_{s,t}) \rangle \propto x_{s,t}^{-\eta_{s,t}}$ at criticality, with the exponent taking the appropriate value depending on whether the displacement x is timelike or spacelike. The ratio $\eta_s/\eta_t > 1$ if $\nu_s/\nu_t < 1$ and *vice versa*. However, η_s/η_t may be identified with the dynamical critical exponent z characterising the quantum critical point, in the sense that the dynamics remains invariant under the scale transformation $\vec{x} \rightarrow \ell\vec{x}$; $x_0 \rightarrow \ell^z x_0$. By considering the anomalous dimension of the Fermi velocity using the $1/N_f$ expansion, Son [5] has obtained $z < 1$, which has implications for the stability of the quasiparticle excitations. If we assume that the same critical exponent governs both quasiparticle and order parameter correlations, then reconciling the two calculations requires an unusually large value of γ .

Next, we set N_f to the physical value 2 and studied the chiral order parameter as a function of coupling strength. Here our results are harder to interpret; we observe a crossover from strong- to weak-coupling behaviour at $1/g^2 \simeq 0.75$, but were unable to model the equation of state, leaving the nature of the weak-coupling regime unclear. There is evidence, both from the large finite volume effects and the curvature in $\langle \bar{\chi}\chi(m) \rangle$, for strong correlations. Work is currently in progress to study the quasiparticle propagator in order to explore the dispersion relation and expose any quantum critical behaviour from an independent direction, and also to further investigate the nature of the fluctuations in the weak-coupling phase at $N_f = 2$.

5 Acknowledgements

SJH thanks the Galileo Galilei Institute for Theoretical Physics for hospitality and the INFN for partial support during the completion of this work.

References

- [1] K. S. Novoselov *et al.*, Nature **438** (2005) 197.
- [2] G.W. Semenoff, Phys. Rev. Lett. **53** (1984) 2449.
- [3] V.P. Gusynin, S.G. Sharapov and J.P. Carbotte, Int. J. Mod. Phys. B **21** (2007) 4611.
- [4] M. Creutz, JHEP **0804**, 017 (2008).
- [5] D.T. Son, Phys. Rev. B **75** (2007) 235423.
- [6] J.E. Drut and D.T. Son, Phys. Rev. B **77** (2008) 075115.
- [7] L. Del Debbio, S.J. Hands and J.C. Mehegan, Nucl. Phys. B **502** (1997) 269.
- [8] L. Del Debbio and S.J. Hands, Nucl. Phys. B **552** (1999) 339;
S.J. Hands and B. Lucini, Phys. Lett. B **461** (1999) 263.
- [9] S. Christofi, S.J. Hands and C. Strouthos, Phys. Rev. D **75** (2007) 101701.
- [10] C.J. Burden and A.N. Burkitt, Europhys. Lett. **3** (1987) 545.
- [11] S.A. Gottlieb, W. Liu, D. Toussaint, R.L. Renken and R. L. Sugar, Phys. Rev. D **35**, 2531 (1987).
- [12] K. Binder and J.-S. Wang, J. Stat. Phys. **55** (1989) 87.
- [13] I.M. Barbour, N. Psycharis, E. Focht, W. Franzki and J. Jersák, Phys. Rev. D **58**, 074507 (1998).